TESTING PLANETARY SUBSURFACE ICE CHARACTERIZATION USING L-BAND RADAR DATA AT THE ASKJA, ICELAND ANALOG SITE. A. D. Johantges[1], D. M. H. Baker[2], J. A. Richardson[2], E. S. Shoemaker[3], S. P. Scheidt[2,5], P. L. Whelley[2,4], and K. E. Young[2]. [1]Dept. of Geography & Env. Engineering, United States Military Academy, West Point, NY 10996 (adam.johantges@westpoint.edu), [2]Solar System Exploration Division, NASA Goddard Space Flight Center, Greenbelt, MD 20771 (david.m.hollibaughbaker@nasa.gov), [3]Lunar and Planetary Laboratory, Univ. of Arizona, Tucson, AZ 85721, [4]Dept. of Astronomy, Univ. of Maryland, College Park, MD 20742, [5]Dept. of Physics and Astronomy, Howard University, Washington, D.C. 20059.

Introduction: Identifying and characterizing the locations of shallow (0–10 m) subsurface ice on the Moon and Mars is important for addressing high-priority science and human exploration objectives [1,2]. Measurements from radar systems, including orbital polarimetric Synthetic Aperture Radar (SAR) and follow-on ground-penetrating radar (GPR) instruments will be critical for characterizing ice deposits and any dry overburden. For example, the Mars Ice Mapper mission concept will carry an L-band SAR to search for subsurface ice at possible human landing sites in the mid to low latitudes of Mars [3].

This study uses aerial and field-based optical and radar imagery and ground observations of a planetary analog site at the Askja Caldera in Northern Iceland to test methods for detecting and characterizing subsurface ice layers. Specifically, we use decompositions of Uncrewed Aerial Vehicle Synthetic Aperture Radar UAVSAR L-band SAR images combined with Uncrewed Aerial System (UAS) -derived orthomosaics and digital elevation models (DEMs) and field observations to understand the scattering behavior of the SAR signal that may indicate ice. For example, as observed on multiple planetary bodies, thick subsurface ice can lead to double-bounce scattering behavior that may lead to high circular polarization ratios and double bounce enhancements in decompositions such as m-chi [4,5]. However, high surface roughness and large blocks or scatterers at the scale of the radar wave can also lead to similar signatures [4-6]. Discriminating between these scattering regimes will be critical for successfully meeting future mission science and exploration objectives.

Field Location and Buried Ice: Buried ice layers were formed within the caldera of the Askja central volcano when eruptions in 1875 and 1961 deposited pyroclasts on fresh snowfall that then densified into solid ice. Ice deposits are located under decimeters to meters of pumice ("1875 pumice") and basaltic ash and lapilli ("1961 scoria") and are ~0.5 to 3 m in thickness [7-8].

Data and Methods: We used publicly available quad-polarized L-band (λ=24 cm) airborne radar data from the UAVSAR instrument (May 2015 observation) at ~5x6 m/pixel resolution. An orthoimage mosaic (1.9 cm/pixel) and a DEM (3.7 cm/pixel resolution) were produced for the Askja caldera study area and a non-ice control site on the 1961 Vikrahraun lava flow using a Mavic 2 Pro quadcopter. Images collected by the quadcopter in August 2019 were processed using AgiSoft Metashape software.

UAVSAR products: We used MapReady software and IDL scripts to calculate the circular polarization ratio (CPR) and m-chi decomposition from ground-projected complex cross product data following [5,6].

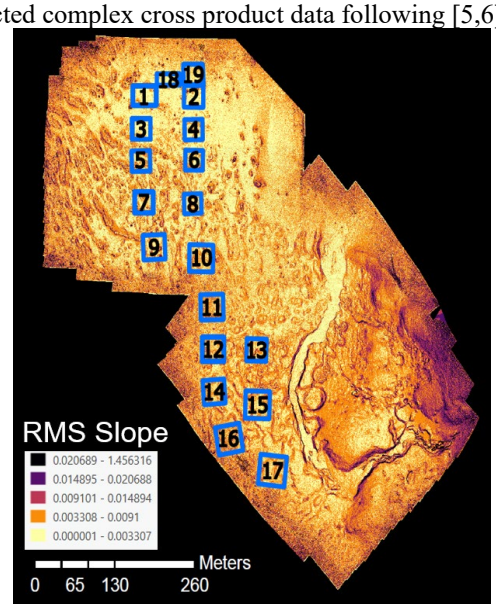

Terrain Roughness: Roughness was calculated from the UAS DEM using the root-mean-square (RMS) slope parameter [9] (Fig. 1) at a one-pixel horizontal baseline (3.7 cm). RMS slope is defined as the square root of the sum of squared differences between a center pixel and all surrounding pixels for every pixel within the DEM. These values are then divided by the horizontal baseline.

Surface units: General classification of optical reflectance-based surface units (e.g., scoria, pumice, rocky lavas, thermokarst) was achieved using an IsoCluster Unsupervised Classification on the UAS Orthoimage.

A total of 18 regions of interest (ROIs) approximately 30 by 30 m in size were selected to represent a variety of unit types within the bounds of the

UAS DEM (Fig. 1); 7 ROIs were selected within the non-ice lava flow site. The ArcGIS Zonal Statistics tool was used to extract the mean and standard deviation of RMS slope and CPR values within each ROI.

Results: The ROIs within the Askja caldera show a range of RMS slope and CPR values (Fig. 2). CPR values are moderate to high, ranging from mean values of 0.40 to 0.69. Standard deviations are high, typically at 0.2, which indicates significant variation within a single ROI. CPR values do not trend with the RMS slope at the 3.7 cm baseline suggesting that other scattering variables may be more dominant at smaller scales. The CPR values within the caldera are also higher than those of the Vikrahraun lava flow (non-ice location), despite its higher surface roughness (Fig. 2).

Discussion: Based on the CPR and roughness values, ROI 3 shows the strongest signature of subsurface ice. This is due to its high CPR values and its relatively low roughness located in the 1961 scoria deposit that consists of few large scatterers; these two variables are not likely to significantly contribute to the elevated CPR values. Furthermore, ROI 3 has an elevated double bounce signature in m-chi decomposition with little volumetric or single scattering components. Indeed, 2021 field observations (trenches and GPR data) confirmed the presence of subsurface ice at this location, occurring at 40 cm depth and thickness of approximately 50-100 cm.

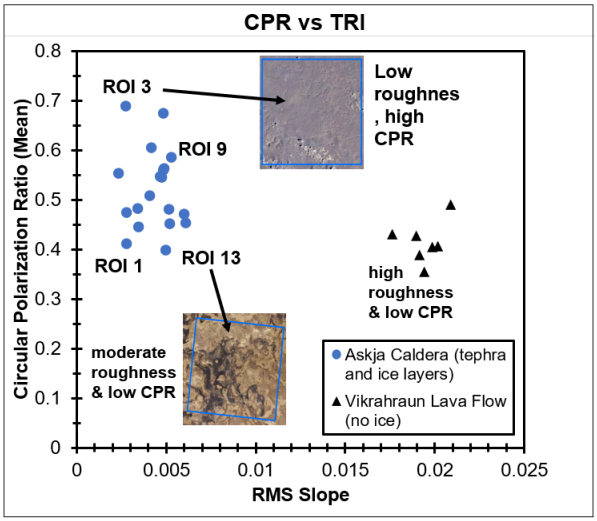

Fig. 2. CPR versus RMS Slope values for 18 ROIs over different surface units inside the Askja caldera and 7 ROIs over the Vikrahraun lava flow. Inset images are UAS orthomosaics showing examples of candidate ice locations with low roughness within the 1961 scoria (ROI 3, 30x30m) and rough thermokarst terrain within 1875 pumice that complicates interpretation of the CPR signal (ROI 13, 30x30).

In other areas with elevated CPR and confirmed presence of ice in the field, the scattering behavior may be due to both subsurface ice layers and topographic roughness, which may complicate interpretation based on radar data alone. For example, in ROI 13 roughness from thermokarst depressions at larger horizontal baselines observed in the UAS orthoimage and DEM and large (>10 cm) pumice fragments at the surface to ~75 cm depth likely contribute to enhanced double bounce and volumetric scattering. This is supported by the m-chi decomposition, which show both volumetric and double bounce components.

Other regions of lower CPR values could result from an absence of ice or decreased roughness, including surface objects such as rocks, cracks, or other facets that detract from the true surface roughness of the soil.

Implications and Future Work: Successfully identifying candidate subsurface ice locations with the circular polarization ratio at L-band frequencies requires additional polarimetric decomposition methods and roughness characterization to understand the radar scattering behavior. Rough areas (e.g., abundant rocks and thermokarst landforms) complicate detection of buried ice and require more information or models to accurately determine the ice and subsurface characteristics. Smooth areas with few internal scatterers in the tephra overburden allow for effective penetration of the radar signal and result in CPR values that are indicative of ice. This workflow can serve as a prerequisite for future subsurface ice detection studies, as it was used in the 2021 NASA Goddard Instrument Field Team Campaign.

Future work will continue testing SAR techniques for subsurface ice detection, including assessing: 1) roughness trends at different baselines and with detrending methods, 2) m-chi and other decomposition products, and 3) the effect of viewing geometries.

Acknowledgments: This work was supported by the NASA Goddard Instrument Field Team (GIFT) Internal Scientist Funding Model (ISFM).

References: [1] MEPAG ICE-SAG Final Report (2019) http://mepag.nasa.gov/reports.cfm. [2] LEAG (2016) The Lunar Exploration Roadmap, https://www.lpi.usra.edu/leag/roadmap/. [3] Watzin J. and Haltigin, T. (2020). Mars Exploration Ice Mapper, presented at April 2020 MEPAG meeting, https://mepag.jpl.nasa.gov/meetings.cfm. [4] Carter et al. (2011) Proceedings of the IEEE, 99(5), 770-782. [5] Raney et al. (2012) JGR 117, E00H21. [6] Neish et al. (2017) *Icarus* 281, 73–89. [7] Richardson, J.A. et al. (2020) LPSC 51, no. 2326. [8] Baker, D.M.H. et al. (2021) LPSC 52, no. 2548. [9] Shepard, M.K. et al. (2001) JGR 106, 32,777-32,795.